Size and shape of excluded volume polymers confined between parallel plates

Debasish Chaudhuri* and Bela Mulder†
FOM Institute AMOLF, Science Park 104, NL-1098 XG Amsterdam, The Netherlands
(Received 3 July 2010; revised manuscript received 1 November 2010; published 18 March 2011)

A number of recent experiments have provided detailed observations of the configurations of long DNA strands under nano-to-micrometer-sized confinement. We therefore revisit the problem of an excluded volume polymer chain confined between two parallel plates with varying plate separation. We show that the nonmonotonic behavior of the overall size of the chain as a function of plate separation, seen in computer simulations and reproduced by earlier theories, can already be predicted on the basis of scaling arguments. However, the behavior of the size in a plane parallel to the plates, a quantity observed in recent experiments, is predicted to be monotonic, in contrast to the experimental findings. We analyze this problem in depth with a mean-field approach that maps the confined polymer onto an anisotropic Gaussian chain, which allows the size of the polymer to be determined separately in the confined and unconfined directions. The theory allows the analytical construction of a smooth crossover between the small-plate-separation de Gennes regime and the large-plate-separation Flory regime. The results show good agreement with molecular dynamics simulations in the presence of a Langevin heat bath and confirm the scaling predictions.

DOI: 10.1103/PhysRevE.83.031803 PACS number(s): 82.35.Lr, 36.20.Ey, 87.15.−v

I. INTRODUCTION

With the typical length scales in cells ranging from tens of nanometers to tens of microns, their polymeric constituents are often spatially constrained. Some of the prominent examples are the cytoskeletal filamentous protein aggregates microtubules and F-actin, which can have lengths up to tens of microns. Recent studies on microtubules in plant cells [1], DNA packaging in viral capsids [2], and DNA segregation in bacterial cell division [3–6] focused on properties of biopolymers strongly influenced by confining geometries. This has naturally led to increased interest in understanding the physics of strongly confined polymers. Among all the polymeric constituents of cells, DNA with its relatively low bending stiffness in comparison to its extremely long length has a special place as it can under most circumstances be described as an classical excluded volume polymer [7]. Important examples of confined DNA are (i) chromosomal DNA that can have bare lengths up to centimeters trapped inside the cell nucleus of a size in the range 1–10 μm, (ii) bacterial DNA of lengths between 0.1 and 100 μm trapped within a small bacterial volume, which for the case of *E. coli* is about 2 μm long and 0.5 μm in diameter, and (iii) mitochondrial DNA of length about 5 μm for human beings with the available mitochondrial size between 0.5 and 10 μm. The combined effects of confinement, self-avoidance, and entropic forces act together in deciding the structure and properties of confined polymers.

A number of single-molecule fluorescence microscopy studies have recently investigated the structure and dynamics of confined DNA trapped between parallel plates [8–11] or within cylindrical geometries [12–14], with the confining dimensions typically of the order of, or smaller than, the bulk radius of gyration of the polymer. In particular, Bonthuis *et al.* [10] have recently observed DNA confined to parallel-plate nanochannels, showing among other things an interesting nonmonotonic variation of the two-dimensional (2D) projected radius of gyration with the distance between channel walls.

Theoretical analyses of confined excluded volume chains already have a long history, encompassing a number of different techniques and approaches such as scaling theories [15,16], renormalization group methods [17–19], computer simulations [8,20–24], and mean-field theory (MFT) [25]. The qualitative picture that emerges from these analyses is simple: With increased degree of confinement, the polymer size shrinks in the confining direction(s) and expands in the nonconfined direction(s). The expansion in the nonconfined directions is due to the excluded volume repulsion between different polymer segments. According to de Gennes' scaling theory [15], this expansion in the strongly confined regime has a power-law dependence on the length scale of the confinement. On the other hand, in the limit of very weak or no confinement the polymer is expected to behave as a free excluded volume polymer approximately obeying the Flory relationship between polymer length and spatial size in three dimensions [7].

Monte Carlo (MC) simulations of self-avoiding lattice random walks trapped within reflecting walls have validated the de Gennes scaling predictions [20,21]. These simulations also showed a nonmonotonic variation of the mean size of the polymer, measured as the full three-dimensional (3D) radius of gyration, as a function of the interwall separation [20]. This nonmonotonicity in the radius of gyration was later also captured by a MFT calculation [25]. Recent experiments on confined DNA [10,11] found nonmonotonicity in the projected 2D size of the polymer, rather than its 3D average. This is in contradiction to de Gennes scaling prediction of a monotonic increase of polymer size parallel to the plates with reduced plate separation. To correctly interpret these results we need a theoretical approach that explicitly allows us to consider the behavior of the polymer in the confined and nonconfined directions separately.

Here we revisit the problem of an excluded volume polymer confined between two parallel plates with the latter

*chaudhuri@amolf.nl
†mulder@amolf.nl

desideratum in mind. By reviewing the extant scaling approaches, we show that the nonmonotonicity of the 3D radius of gyration with plate separation already follows from a scaling analysis if due care is given to the details of its application. We then construct a MFT for the confined polymer that goes beyond the existing theory, in that it explicitly takes into account the symmetry breaking induced by the confinement in the construction of the noninteracting reference polymer. The MFT agrees with de Gennes scaling at smallest plate separations and Flory scaling in the limit of large plate separations, and allows the analytical determination of the prefactors of the scaling relations. Moreover, this approach allows for calculation of corrections to de Gennes scaling for intermediate plate separations. Our main result is that the size of the polymer transverse to the confining direction, i.e., parallel to the confining planes, grows *monotonically* with decreasing separation between the plates, even after incorporating corrections to de Gennes scaling. The results of the MFT approach are then validated by an explicit off-lattice simulation of a confined polymer. The nonmonotonicity of the 3D radius of gyration therefore is due to the fact that, with decreasing plate separation, initially the polymer size in the confining direction decreases more rapidly than it grows in the unconfined directions, and eventually the latter becomes dominant.

The paper consists of three main sections. We begin with by describing the existing scaling approaches in Sec. II. In Sec. III we present our self-consistent MFT calculation and its predictions. In Sec. IV we describe the molecular dynamics simulation scheme and compare the results with our MFT predictions. Finally we conclude in Sec. V by summarizing our results and providing an outlook. Several appendices collect some of the more technical material.

II. SCALING THEORIES

In this section, we briefly review the existing scaling theories for a polymer confined between parallel plates. We show that the nonmonotonicity of the mean polymer size as a function of the plate separation, as observed in earlier simulations [20], is in fact intrinsic to de Gennes scaling predictions.

The first scaling theory of self-avoiding polymer behavior is due to Flory. Because of their simplicity Flory-like arguments have been extended to other cases, e.g., semiflexible polymers [26]. Within Flory scaling theory the free energy of an excluded volume polymer in d dimensions can be written as [27]

$$\beta F \sim \frac{R^2}{N l^2} + l^d \frac{N^2}{R^d},$$

where R is the end-to-end distance of the polymer constructed of N segments, each of size l, $\beta = 1/k_B T$, with k_B the Boltzmann constant and T the ambient temperature. The first term describes the entropic elasticity of a free chain, and the second term describes the repulsive interaction between different segments. Minimizing the free energy with respect to R one obtains the Flory estimate of the equilibrium polymer size $R \sim N^{3/(d+2)} l$. As de Gennes pointed out [7], the success of Flory's theory relies on remarkable cancellation of overestimates in both the terms. For polymers confined between parallel plates, a Flory-like argument predicts an equilibrium polymer size in the unconfined directions that agrees with de Gennes scaling (which we discuss next), but the free energy it predicts is not extensive in N [23].

The de Gennes scaling arguments for the size of a polymer confined between parallel plates can be described as follows [15]. If the plate separation $D \lesssim L = N l$ the polymer contour length, the size of the polymer in the confining direction (perpendicular to the confining plates), $R_\perp$, becomes limited by the confinement, so that $R_\perp \sim D$. The size of the polymer in the unconfined directions (parallel to the confining plates), $R_\parallel$, should be entirely decided by the following two length scales: the 3D Flory size of a polymer $R \sim N^{3/5} l$ and the plate separation D. Thus $R_\parallel = R\,\phi(R/D)$, so that $\phi(x) = 1$ when $x \to 0$ (3D Flory regime) and $\phi(x) \sim x^q$ when $x > 1$ (de Gennes regime). In the 2D limit ($x \gg 1$) Flory scaling requires $R_\parallel \sim N^{3/4} l$. This ensures $q = 1/4$ and therefore $R_\parallel \sim N^{3/4}(l/D)^{1/4} l$. This power-law divergence of $R_\parallel$ with decreasing D was observed in MC simulations of self-avoiding lattice random walks [20,21] and also in recent experiments on confined DNA [10,11]. The excess free energy measured from the state of an unconfined self-avoiding polymer can be expressed [15] as $\beta F = \psi(R/D)$, so that $\psi(x) = 0$ for $x \to 0$ and $\psi(x) = x^p$ in the other limit of small D. Demanding that the excess free energy has to be an extensive function of N one obtains $p = 5/3$ and $\beta F \sim N(l/D)^{5/3}$.

We notice that, in terms of plate separation D, de Gennes scaling predicts two completely opposite behaviors for $R_\perp \sim D$ and $R_\parallel \sim N^{3/4}(l/D)^{1/4} l$. While $R_\perp$ *decreases*, $R_\parallel$ *increases* with decreasing D. Therefore, the mean size of the polymer, averaged over all the three directions, $R_{\rm tot}^2 = R_\perp^2 + 2R_\parallel^2 \sim a_1 D^2 + a_2 D^{-1/2}$ (a_1, a_2 are positive constants), is expected to vary nonmonotonically with D. The $R_{\rm tot}^2 \sim D^{-1/2}$ behavior at very small D crosses over to $R_{\rm tot}^2 \sim D^2$ at moderately large D via a minimum in $R_{\rm tot}^2$. This fact is illustrated in Fig. 1 and was observed in previous simulations [20]. At large $D(\gg L)$, the scaling function $\phi(R/D) = 1$, and therefore the average size $R_{\rm tot}^2$ becomes independent of D (Fig. 1).

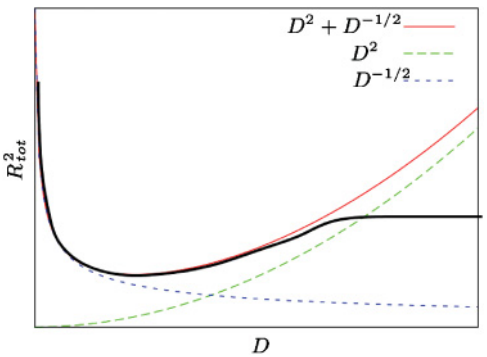

FIG. 1. (Color online) Schematic diagram of the nonmonotonic behavior of average polymer size $R_{\rm tot}^2 \sim a_1 D^2 + a_2 D^{-1/2}$ (dark thick line). In the limit of small $D(\lesssim L$ contour length), the combination of D^2 and $D^{-1/2}$ behavior of the polymer size in the confining and orthogonal directions, respectively, leads to nonmonotonicity with a clear minimum in the average polymer size $R_{\rm tot}^2$. At large $D(> L)$, $R_{\rm tot}^2$ crosses over to the Flory regime and becomes independent of D.

It should be noted here that this behavior is not the same as the nonmonotonicity observed in experimental measurement of the parallel component of the radius of gyration of a DNA confined between parallel plates [10,11]. De Gennes scaling predicts a clear monotonic increase of the component $R_\parallel$ with shrinking D.

It is instructive to compare this behavior with that of an ideal chain confined between parallel plates. For an ideal chain, in absence of any interaction, the impact of the confinement remains restricted to the confining direction only. Thus $R_\perp \sim D$ for small D and $R_\perp \sim N^{1/2}l$ in the bulk limit.

However, $R_\parallel \sim N^{1/2}l$ is obeyed independently of D. Therefore the overall size is $R_{\rm tot}^2 \sim a_3 D^2 + 2R_\parallel^2$ with a_3 a positive constant. Starting from the bulk value, with shrinking D, $R_{\rm tot}^2$ reduces to ultimately saturate at $2R_\parallel^2$. The initial reduction of overall size is thus common to both ideal polymers and excluded volume polymers. However, the expansion of the overall polymer size with further reduction of D for excluded volume polymers is a signature of the repulsion between polymer segments.

III. MEAN FIELD THEORY

A. Overview

The starting point for our MFT is a description of the polymer as a space curve $\mathbf{r}(s)$, in which s is the arc length parameter with domain $0 \leqslant s \leqslant L$. The energetics of the excluded volume (i.e., self-avoiding) polymer is given by the Edwards Hamiltonian [28]

$$\beta\mathcal{H} = \frac{3}{2l}\int_0^L ds \left[\frac{\partial \mathbf{r}(\mathbf{s})}{\partial s}\right]^2 + \frac{1}{2}b\int_0^L ds \int_0^L ds'\, \delta[\mathbf{r}(\mathbf{s}) - \mathbf{r}(\mathbf{s}')]. \quad (1)$$

The parameter b sets the strength of the repulsive intersegment interactions.

Edwards and Singh [28] first proposed to determine the size of a free self-avoiding polymer by mapping it onto an isotropic Gaussian chain with reference Hamiltonian

$$\beta\mathcal{H}_{\rm iso} = \frac{3}{2l_0}\int_0^L ds \left[\frac{\partial \mathbf{r}(\mathbf{s})}{\partial s}\right]^2,$$

and then choosing the effective segment size l_0 self-consistently by requiring the first-order variation of the mean-squared end-to-end distance $\langle R^2\rangle$ in the interaction parameter b to vanish. This approach relatively simply reproduces the Flory result $R \sim N^{\frac{3}{5}}$ for the scaling of polymer size with polymer length. This same idea was later applied by Thirumalai and co-workers [25,29] to confined polymers. In the latter approach one first imposes the confinement on an isotropic Gaussian reference chain and then performs a self-consistent calculation to determine effective segment length of the reference chain.

The scaling analysis presented in the previous section, however, shows that in order to understand the behavior of the confined chain one has to be able to separately address the effect of the confinement on the longitudinal and perpendicular size of the polymer. Moreover, on formal grounds one can pose the question whether an *isotropic* ideal reference chain is appropriate to the situation where the presence of the boundaries already explicitly breaks the bulk rotational symmetry. Here we propose that both these challenges can be met by mapping the confined polymer onto an *anisotropic* reference chain, composed of bonds whose length depends on their absolute orientation with respect to the uniaxial symmetry axis of the confining geometry perpendicular to the boundary planes. Such an anisotropic Gaussian reference chain is described by the Hamiltonian

$$\beta\mathcal{H}_0 = \frac{3}{2l_\parallel}\int_0^L ds \left[\frac{\partial \mathbf{r}_\parallel(s)}{\partial s}\right]^2 + \frac{3}{2l_\perp}\int_0^L ds \left[\frac{\partial r_\perp(s)}{\partial s}\right]^2 \equiv \beta\mathcal{H}_\parallel + \beta\mathcal{H}_\perp. \quad (2)$$

The two effective segment lengths $l_\parallel$ and $l_\perp$ are now the parameters that have to be determined self-consistently. Apart from the fact that this choice is physically plausible given the geometry of the system and allows independent predictions for the behavior of the polymer in the parallel and transverse directions with respect to the confinement, it has another potential advantage in that generically multiparameter MFTs can be expected to yield better approximations to the underlying physics than single-parameter ones. This is brought into clear focus when one considers that this two-parameter theory reduces to the one presented in Ref. [25] when one imposes the identity $l_\parallel = l_\perp$ from the outset, for which there are few *a priori* arguments, except possibly parsimony.

As an aside, it should be noted that although Ref. [25] described their approach as a variational MFT, it, its predecessor Ref. [28], and our further generalization are not variational in the sense of following from the minimization of an appropriate free energy functional; rather, they constitute attempts to determine the properties of the polymer self-consistently on the basis of constraints imposed on a single or two moments of the chain configuration distribution. Arguably, a "true" MFT would in fact condition on a necessarily infinite, complete set of moments of the full distribution.

We assume the z axis of our coordinate system to be perpendicular to the confining planes. For convenience, we consider the lateral extent of the system to be finite, defined by a length $W \gg D$, but freely take the limit of an infinite extent wherever appropriate. The hard-wall confinement is implemented through the Dirichlet boundary condition by which the Green's function corresponding to the reference Hamiltonian vanishes at the two confining walls. The full Hamiltonian can be expressed as

$$\beta\mathcal{H} = \beta\mathcal{H}_0 + \beta\Delta\mathcal{H}_\parallel + \beta\Delta\mathcal{H}_\perp + \beta\Delta\mathcal{H}_b, \quad (3)$$

where

$$\beta\Delta\mathcal{H}_\parallel = \frac{3}{2}\left(\frac{1}{l} - \frac{1}{l_\parallel}\right)\int_0^L ds \left[\frac{\partial \mathbf{r}_\parallel(s)}{\partial s}\right]^2, \quad (4)$$

$$\beta\Delta\mathcal{H}_\perp = \frac{3}{2}\left(\frac{1}{l} - \frac{1}{l_\perp}\right)\int_0^L ds \left[\frac{\partial r_\perp(s)}{\partial s}\right]^2, \quad (5)$$

$$\beta\Delta\mathcal{H}_b = \frac{1}{2}b\int_0^L ds \int_0^L ds'\, \delta[\mathbf{r}(\mathbf{s}) - \mathbf{r}(\mathbf{s}')] \quad (6)$$

are treated as perturbative corrections.

Statistical averages with respect to the Hamiltonian $\mathcal{H}$ are defined through a path integral

$$\langle A[\mathbf{r}(s)]\rangle = \frac{1}{Z_{\mathcal{H}}}\int d\mathbf{r}(0)\int d\mathbf{r}(L) \times \int_{\mathbf{r}(0)}^{\mathbf{r}(L)} \mathcal{D}[\mathbf{r}(s)]A[\mathbf{r}(s)]\exp\{-\beta\mathcal{H}[\mathbf{r}(s)]\}, \quad (7)$$

where the normalization constant is given by the partition function

$$Z_{\mathcal{H}} = \int d\mathbf{r}(0)\int d\mathbf{r}(L)\int_{\mathbf{r}(0)}^{\mathbf{r}(L)}\mathcal{D}[\mathbf{r}(s)]\exp\{-\beta\mathcal{H}[\mathbf{r}(s)]\}. \quad (8)$$

We now consider the components of the end-to-end separation $\mathbf{R}_\parallel = \mathbf{r}_\parallel(L) - \mathbf{r}_\parallel(0)$ and $R_\perp = r_\perp(L) - r_\perp(0)$ and the averages $\langle R_\parallel^2\rangle$ and $\langle R_\perp^2\rangle$.

Expanding the Hamiltonian $\mathcal{H}$ in the above expression up to linear order in $\Delta\mathcal{H}$ around the reference Hamiltonian $\mathcal{H}_0$, we obtain

$$\langle R_\parallel^2\rangle = \langle R_\parallel^2\rangle_0 - \delta_\parallel + \mathcal{O}(\Delta\mathcal{H}^2), \quad (9)$$

$$\langle R_\perp^2\rangle = \langle R_\perp^2\rangle_0 - \delta_\perp + \mathcal{O}(\Delta\mathcal{H}^2), \quad (10)$$

where

$$\begin{aligned}\delta_\parallel &= \{\langle R_\parallel^2\beta\Delta\mathcal{H}_\parallel\rangle_0 - \langle R_\parallel^2\rangle_0\langle\beta\Delta\mathcal{H}_\parallel\rangle_0\} \\ &\quad +\{\langle R_\parallel^2\beta\Delta\mathcal{H}_\perp\rangle_0 - \langle R_\parallel^2\rangle_0\langle\beta\Delta\mathcal{H}_\perp\rangle_0\} \\ &\quad +\{\langle R_\parallel^2\beta\Delta\mathcal{H}_b\rangle_0 - \langle R_\parallel^2\rangle_0\langle\beta\Delta\mathcal{H}_b\rangle_0\} \\ &\equiv \delta_\parallel^\parallel + \delta_\parallel^\perp + \delta_\parallel^b, \quad (11)\\ \delta_\perp &= \{\langle R_\perp^2\beta\Delta\mathcal{H}_\parallel\rangle_0 - \langle R_\perp^2\rangle_0\langle\beta\Delta\mathcal{H}_\parallel\rangle_0\} \\ &\quad +\{\langle R_\perp^2\beta\Delta\mathcal{H}_\perp\rangle_0 - \langle R_\perp^2\rangle_0\langle\beta\Delta\mathcal{H}_\perp\rangle_0\} \\ &\quad +\{\langle R_\perp^2\beta\Delta\mathcal{H}_b\rangle_0 - \langle R_\perp^2\rangle_0\langle\beta\Delta\mathcal{H}_b\rangle_0\} \\ &\equiv \delta_\perp^\parallel + \delta_\perp^\perp + \delta_\perp^b. \quad (12)\end{aligned}$$

Here $\langle\cdots\rangle_0$ indicates a statistical average taken with respect to the reference Hamiltonian $\mathcal{H}_0$. In the above expressions, $\delta_\parallel^\parallel$, $\delta_\parallel^\perp$, $\delta_\perp^\perp$, and $\delta_\perp^\parallel$ are the corrections due to the chain anisotropy, and $\delta_\parallel^b$ and $\delta_\perp^b$ are the corrections from excluded volume interactions. The MFT approximation requires a choice of $l_\parallel$ and $l_\perp$ so that $\langle R_\parallel^2\rangle = \langle R_\parallel^2\rangle_0$ and $\langle R_\perp^2\rangle = \langle R_\perp^2\rangle_0$. Thus, solving $\delta_\parallel = \delta_\perp = 0$, one can obtain the effective segment lengths $l_\parallel$ and $l_\perp$ in terms of plate separation D, contour length L, and intersegment interaction strength b.

Reference [28] obtained Flory scaling within corrections up to linear order in $\beta\Delta\mathcal{H}$. The inclusion of higher-order terms was shown to change the coefficients of scaling form, however, keeping them stable [28]. We expect the same to hold in the present problem as well [25], as the nature of interactions used here is exactly the same.

We now briefly summarize the main results we obtained using this MFT. In the limit of very large plate separations ($D \to \infty$) the system becomes isotropic with

$$l_\parallel = l_\perp \equiv l_B \sim (bl)^{2/5}L^{1/5}, \quad (13)$$

and the mean-squared end-to-end separation follows the relation

$$\langle R^2\rangle = Ll_B \sim (bl)^{2/5}L^{6/5}, \quad (14)$$

which is independent of D and obeys Flory scaling.

In the limit of strong confinement ($D \to 0$),

$$l_\perp \simeq \frac{l}{2}\left(1+\sqrt{1-\frac{4bD}{ll_\parallel}}\right) \simeq l - \frac{4\sqrt{2\pi}}{3}\sqrt{\frac{b}{l}}\frac{D^{3/2}}{L^{1/2}}, \quad (15)$$

$$l_\parallel \simeq \frac{l}{2}\left(1+\sqrt{1+\frac{9b}{2\pi l}\frac{L}{D}}\right) \simeq \frac{3}{2\sqrt{2\pi}}\sqrt{bl}\sqrt{\frac{L}{D}}. \quad (16)$$

Using these, we obtain the size of the polymer in the confining direction

$$\langle R_\perp^2\rangle \simeq \left(1-\frac{8}{\pi^2}\right)\frac{D^2}{2} - \frac{D^2}{8}e^{-3\kappa L} \quad (17)$$

with $\kappa = (1/6)l_\perp(\pi/D)^2$, and in the unconfined directions

$$\begin{aligned}\langle R_\parallel^2\rangle &\simeq \frac{1}{3}Ll\left(1+\sqrt{1+\frac{9b}{2\pi l}\frac{L}{D}}\right) \\ &\sim \sqrt{\frac{1}{2\pi}}(bl)^{1/2}L^{3/2}D^{-1/2}. \quad (18)\end{aligned}$$

With shrinking plate separation D the polymer gets compressed in the confining direction and expands in the free directions. Up to the leading order (in the small D limit) $\langle R_\perp^2\rangle \sim D^2$ and $\langle R_\parallel^2\rangle \sim L^{3/2}D^{-1/2}$ obeying de Gennes scaling. Beyond the leading order, the expressions we found describe a smooth crossover to large D behavior (see Fig. 2).

We now present a detailed derivation of the Eqs. (13)–(18).

B. Formulation

1. Green's function

In order to determine all the above mentioned averages, we require the Green's function corresponding to the anisotropic reference Hamiltonian $\mathcal{H}_0$ [Eq. (2)] defined as

$$G_0(\mathbf{r},L|\mathbf{r}',0) = \int_{\mathbf{r}'=\mathbf{r}(0)}^{\mathbf{r}=\mathbf{r}(L)}\mathcal{D}[\mathbf{r}(s)]\exp\{-\beta\mathcal{H}_0[\mathbf{r}(s)]\}. \quad (19)$$

The Green's function obeys the following differential equation [30]:

$$\left(\frac{\partial}{\partial L} - \frac{l_\parallel}{6}\nabla_\parallel^2 - \frac{l_\perp}{6}\frac{d^2}{dz^2}\right)G_0 = 0. \quad (20)$$

Using the Dirichlet boundary condition in the confining direction $G_0(z=0,D)=0$ and free boundary condition in the unconfined directions (along the x and y axes), one obtains a variable separable form of the Green's function (see Appendix A)

$$G_0 = G_\parallel(\mathbf{r}_\parallel,L \mid \mathbf{r}'_\parallel,0)\; G_\perp(r_\perp,L \mid r'_\perp,0), \quad (21)$$

where

$$G_\parallel = \frac{3}{2\pi l_\parallel L}e^{-\frac{3}{2l_\parallel L}(\mathbf{r}_\parallel-\mathbf{r}'_\parallel)^2} \quad (22)$$

and

$$G_\perp = \frac{2}{D}\sum_{n=1}^{\infty}\sin\left(\frac{n\pi}{D}r_\perp\right)\sin\left(\frac{n\pi}{D}r'_\perp\right)e^{-\kappa n^2 L}, \quad (23)$$

with $\kappa = \frac{1}{6}l_\perp(\frac{\pi}{D})^2$.

2. Partition function

The partition function corresponding to the reference Hamiltonian $\mathcal{H}_0$ can also be written in a variable-separable form

$$Z = \int d\mathbf{r}(\mathbf{L})\int \mathbf{dr(0)G_0(r(L),L \mid r(0),0)} = \mathbf{Z}_\parallel \mathbf{Z}_\perp, \quad (24)$$

where

$$Z_\parallel = \int d\mathbf{r}_\parallel \int d\mathbf{r}'_\parallel G_\parallel(\mathbf{r}_\parallel, L \mid \mathbf{r}'_\parallel, 0) = W^2 \quad (25)$$

and

$$Z_\perp = \int dr_\perp \int dr'_\perp G_\perp(r_\perp, L \mid r'_\perp, 0) = \sum_{n=0}^{\infty}\frac{8D}{(2n+1)^2\pi^2}e^{-\kappa L(2n+1)^2}. \quad (26)$$

Remember that W^2 denotes the area of the unconfined xy plane, and we freely take the limit $W \to \infty$ wherever appropriate.

3. End-to-end separation: Contribution from reference Hamiltonian

Using the above mentioned Green's function G_0 one can calculate the end-to-end separations

$$\langle R^2_\parallel\rangle_0 = \frac{\int d\mathbf{r}_\parallel \int d\mathbf{r}'_\parallel(\mathbf{r}_\parallel - \mathbf{r}'_\parallel)^2 G_\parallel(\mathbf{r}_\parallel, L|\mathbf{r}'_\parallel, 0)}{\int d\mathbf{r}_\parallel \int d\mathbf{r}'_\parallel G_\parallel(\mathbf{r}_\parallel, L|\mathbf{r}'_\parallel, 0)} = \frac{2}{3}l_\parallel L \quad (27)$$

and

$$\langle R^2_\perp\rangle_0 = \frac{\int_0^D dr_\perp \int_0^D dr'_\perp (r_\perp - r''_\perp)^2 G_\perp(r_\perp, L|r'_\perp, 0)}{\int_0^D dr_\perp \int_0^D dr'_\perp G_\perp(r_\perp, L|r'_\perp, 0)} = \frac{D^2}{2}\frac{\nu}{\xi}, \quad (28)$$

where

$$\nu = \sum_{n=0}^{\infty}\frac{1}{(2n+1)^2}\left[1 - \frac{8}{(2n+1)^2\pi^2}\right]e^{-\kappa(2n+1)^2 L} - \sum_{n=1}^{\infty}\frac{1}{(2n)^2}e^{-\kappa(2n)^2 L} \quad (29)$$

and

$$\xi = \sum_{n=0}^{\infty}\frac{1}{(2n+1)^2}e^{-\kappa(2n+1)^2 L}. \quad (30)$$

4. End-to-end separation: Corrections from chain anisotropy

We now calculate the first-order contributions $\delta^\parallel_\parallel$, $\delta^\perp_\parallel$, $\delta^\parallel_\perp$ and $\delta^\perp_\perp$ that are due to the anisotropy of the reference chain. Using the definition of the mean-squared end-to-end distance

$$\langle R^2_\parallel\rangle_0 = \frac{\int d\mathbf{r}_\parallel \int d\mathbf{r}'_\parallel(\mathbf{r}_\parallel - \mathbf{r}'_\parallel)^2 \int_{\mathbf{r}'_\parallel=\mathbf{r}_\parallel(0)}^{\mathbf{r}_\parallel=\mathbf{r}_\parallel(L)}\mathcal{D}[\mathbf{r}_\parallel(s)]\exp\{-\beta\mathcal{H}_\parallel[\mathbf{r}(s)]\}}{\int d\mathbf{r}_\parallel \int d\mathbf{r}'_\parallel \int_{\mathbf{r}'_\parallel=\mathbf{r}_\parallel(0)}^{\mathbf{r}_\parallel=\mathbf{r}_\parallel(L)}\mathcal{D}[\mathbf{r}_\parallel(s)]\exp\{-\beta\mathcal{H}_\parallel[\mathbf{r}(s)]\}}$$

along with the identity

$$\beta\mathcal{H}_\parallel[\mathbf{r}(s)] = \alpha_\parallel\frac{2}{3}\left(\frac{1}{l} - \frac{1}{l_\parallel}\right)^{-1}\beta\Delta\mathcal{H}_\parallel[\mathbf{r}(s)],$$

where $\alpha_\parallel = 3/2l_\parallel$, we obtain

$$-\frac{3}{2}\left(\frac{1}{l} - \frac{1}{l_\parallel}\right)\frac{\partial}{\partial\alpha_\parallel}\langle R^2_\parallel\rangle_0 = \{\langle R^2_\parallel\,\beta\Delta\mathcal{H}_\parallel\rangle_0 - \langle R^2_\parallel\rangle_0\langle\beta\Delta\mathcal{H}_\parallel\rangle_0\}$$

$$\text{or} \quad \delta^\parallel_\parallel = \frac{2}{3}\left(\frac{1}{l} - \frac{1}{l_\parallel}\right)Ll^2_\parallel. \quad (31)$$

Similarly, one can show that (with $\alpha_\perp = 3/2l_\perp$)

$$\delta^\perp_\parallel = -\frac{3}{2}\left(\frac{1}{l} - \frac{1}{l_\perp}\right)\frac{\partial}{\partial\alpha_\perp}\langle R^2_\parallel\rangle_0 = 0, \quad (32)$$

$$\delta^\parallel_\perp = -\frac{3}{2}\left(\frac{1}{l} - \frac{1}{l_\parallel}\right)\frac{\partial}{\partial\alpha_\parallel}\langle R^2_\perp\rangle_0 = 0, \quad (33)$$

$$\delta^\perp_\perp = -\frac{3}{2}\left(\frac{1}{l} - \frac{1}{l_\perp}\right)\frac{\partial}{\partial\alpha_\perp}\langle R^2_\perp\rangle_0, \quad (34)$$

where the last derivative can be explicitly evaluated by considering Eq. (28). This leads to the following expression:

$$\delta^\perp_\perp = -\frac{\pi^2}{12\xi}l^2_\perp L\left(\frac{1}{l} - \frac{1}{l_\perp}\right) \times\left\{\sum_{n=0}^{\infty}\left[1 - \frac{8}{(2n+1)^2\pi^2} - \frac{\nu}{\xi}\right]e^{-\kappa L(2n+1)^2} - \sum_{n=1}^{\infty}e^{-\kappa L(2n)^2}\right\}, \quad (35)$$

where ν and ξ are defined by Eqs. (29) and (30), respectively.

5. End-to-end separation: Corrections from excluded volume interactions

Now we evaluate $\delta^b_\parallel$ and $\delta^b_\perp$. Note that the presence of $\delta(\mathbf{r}(\mathbf{s}) - \mathbf{r}(\mathbf{s}'))$ in the self-avoidance interaction $\beta\Delta\mathcal{H}_b$ [Eq. (6)] couples the transverse and the longitudinal modes of the Green's function. This is the term through which $\langle R^2_\parallel\rangle$ becomes dependent on the plate separation D.

The calculation of these two terms are lengthy but straightforward. Here we quote only the final results deferring the details of the calculations to Appendix B:

$$\delta^b_\parallel = -Z^{-1}\frac{b}{\pi}W^2\sum_{n_L,n',n_0=1}^{\infty}M(n_L,n',n_0;\kappa) \times(2\delta_{n_0,n_L} + \delta_{n',(n_0+nL)/2} - \delta_{n',(n_0-nL)/2} - \delta_{n',(nL-n_0)/2})J_0(n_L,n_0), \quad (36)$$

where

$$M(n_L,n',n_0;\kappa) = e^{-\kappa L n_L^2}\int_0^L ds' \int_{s'}^L ds\left(e^{-\kappa s(n'^2-n_L^2)}e^{-\kappa s'(n_0^2-n'^2)}\right), \quad (37)$$

$$J_0(n_L,n_0) = \frac{1}{n_0 n_L \pi^2}[1-(-1)^{n_L}][1-(-1)^{n_0}], \quad (38)$$

and

$$\delta_\perp^b = \frac{b}{Z}W^2\frac{3}{2\pi l_\parallel}\sum_{n_L,n',n_0=1}^{\infty} D^2\,K(n_L,n',n_0;\kappa) \times(2\delta_{n_0,n_L}+\delta_{n',(n_0+nL)/2}-\delta_{n',(n_0-nL)/2}-\delta_{n',(nL-n_0)/2}) \times\left[J(n_L,n_0)-\frac{\langle R_\perp^2\rangle_0}{D^2}J_0(n_L,n_0)\right], \quad (39)$$

where

$$K(n_L,n',n_0;\kappa) = e^{-\kappa L n_L^2}\lim_{a\to 0}\int_0^L ds'\int_{s'}^L ds \times\left[\frac{e^{-\kappa s(n'^2-n_L^2)}e^{-\kappa s'(n_0^2-n'^2)}}{(s-s')+a}\right], \quad (40)$$

$$J(n_L,n_0) = -\frac{1}{n_L^3 n_0\pi^4}\left\{(-1)^{n_L}n_L^2\pi^2+2[1-(-1)^{n_L}]\right\}[1-(-1)^{n_0}] - \frac{2}{n_L n_0\pi^2}(-1)^{n_0}(-1)^{n_L} - \frac{1}{n_L n_0^3\pi^4}\left\{(-1)^{n_0}n_0^2\pi^2+2[1-(-1)^{n_0}]\right\}[1-(-1)^{n_L}]. \quad (41)$$

C. Results

1. Large plate-separation limit: $D\to\infty$

Here we demonstrate that the MFT scheme naturally leads to Flory scaling in the bulk limit of $D\to\infty$. This limit is better appreciated, in a shifted coordinate system in which the confining hard walls are at $z=\pm D/2$. In this coordinate system, the transverse component of Green's function is

$$G_\perp = \frac{1}{D}\sum_{n,\text{even}}\sin\frac{n\pi z'}{D}\sin\frac{n\pi z}{D}e^{-\kappa n^2 L} + \frac{1}{D}\sum_{n,\text{odd}}\cos\frac{n\pi z'}{D}\cos\frac{n\pi z}{D}e^{-\kappa n^2 L}.$$

In the continuum limit of $D\to\infty$

$$G_\perp = \sqrt{\frac{3}{2\pi l_\perp L}}\exp\left[-\frac{3}{2}\frac{(z-z')^2}{l_\perp L}\right]. \quad (42)$$

Here $\delta_\parallel^\parallel$ is independent of D and is given by Eq. (31). The details of the calculation of $\delta_\parallel^b$, $\delta_\perp^b$, and $\delta_\perp^\perp$ in this bulk limit are presented in Appendix C. In this limit the equations, $\delta_\parallel = \delta_\parallel^\parallel+\delta_\parallel^b = 0$ and $\delta_\perp = \delta_\perp^\perp+\delta_\perp^b = 0$ imply

$$\frac{Ll_\parallel^2}{l} \sim \frac{b}{l_\perp^{1/2}}L^{3/2} \quad (43)$$

and

$$\frac{Ll_\perp^2}{l} \sim \frac{bl_\perp^{1/2}}{l_\parallel}L^{3/2}, \quad (44)$$

respectively. Equations (43) and (44) lead to $l_\parallel = l_\perp \equiv l_B$, the isotropy expected in the limit of $D\to\infty$. This also implies

$$l_B \sim (bl)^{2/5}L^{1/5} \quad (45)$$

and

$$\langle R^2\rangle = Ll_B \sim (bl)^{2/5}L^{6/5}, \quad (46)$$

i.e., Flory scaling in three dimensions.

2. Narrow plate-separation limit: $D\to 0$

In the limit of $D\to 0$, $\kappa = l_\perp(\pi/D)^2/6\to\infty$, and only the small n eigenfunctions contribute to the calculation of perturbative corrections to end-to-end distance. The simplest approximation in this limit is the ground-state approximation (only the minimum value of n's contribute).

Ground-state approximation. We first calculate $\delta_\parallel^b$ within the ground-state approximation. Using $n_0 = n' = n_L = 1$, we get $M(1,1,1;\kappa) = (L^2/2)\exp(-\kappa L)$ and $Z = W^2(8D/\pi^2)\exp(-\kappa L)$, which leads to $\delta_\parallel^b = -(3b/4\pi)(L^2/D)$ [using Eq. (36)]. Within MFT, $l_\parallel$ satisfies the condition $\delta_\parallel = \delta_\parallel^\parallel+\delta_\parallel^b = 0$, which implies that

$$\frac{2}{3}\left(\frac{1}{l}-\frac{1}{l_\parallel}\right)Ll_\parallel^2 = \frac{3b}{4\pi}\frac{L^2}{D}.$$

The solution of this equation gives

$$l_\parallel = \frac{l}{2}\left(1+\sqrt{1+\frac{9b}{2\pi l}\frac{L}{D}}\right),$$

which is Eq. (16). Therefore, we find the relation given in Eq. (18):

$$\langle R_\parallel^2\rangle = \frac{2}{3}l_\parallel L = \frac{1}{3}Ll\left(1+\sqrt{1+\frac{9b}{2\pi l}\frac{L}{D}}\right) \sim \sqrt{\frac{1}{2\pi}}(bl)^{1/2}L^{3/2}D^{-1/2}.$$

In the last step, the diverging part of $\langle R_\parallel^2\rangle_0$ in the limit of $D\to 0$ is extracted. Thus, up to the leading order in the limit of $D\to 0$ we find de Gennes scaling $R_\parallel = \sqrt{\langle R_\parallel^2\rangle}\sim(1/\sqrt{2\pi})(bl)^{1/4}L^{3/4}D^{-1/4}$.

Now we calculate the perpendicular component $\langle R_\perp^2\rangle$ within the ground-state approximation $n_L = n' = n_0 = 1$. Thus Eq. (39) reduces to

$$\delta_\perp^b = \frac{9b}{2\pi l_\parallel Z}W^2D^2K(1,1,1;\kappa)\left[J(1,1)-\frac{4}{\pi^2}\frac{\langle R_\perp^2\rangle_0}{D^2}\right].$$

In the expression of $\langle R_\perp^2\rangle_0$ [Eq. (28)] we retain only the $n=0$ terms, within the ground-state approximation, to obtain $\langle R_\perp^2\rangle_0 = 1-8/\pi^2$. This leads to $J(1,1)-(4/\pi^2)\langle R_\perp^2\rangle_0 = 0$ and therefore $\delta_\perp^b = 0$. It can be easily seen that within the ground-state approximation $\delta_\perp^\perp = 0$ too. Thus $l_\perp$ remains

indeterminate. We need to go up to the first excited-state approximation (next higher values of n) to obtain the expression for $l_\perp$.

First excited-state approximation. Within this approximation, we can write Eq. (39) as

$$\delta_\perp^b = \frac{3b}{2\pi l_\parallel Z} W^2 D^2 \left[3K(1,1,1;\kappa)\, T_1 + 2K(1,2,1;\kappa)\, T_1 + 2K(2,1,2;\kappa) T_2 + 3K(2,2,2;\kappa) T_2\right],$$

where

$$T_1 = J(1,1) - \frac{\langle R_\perp^2\rangle_0}{D^2} J_0(1,1) = \frac{1}{2\pi^2} e^{-3\kappa L},$$

$$T_2 = J(2,2) - \frac{\langle R_\perp^2\rangle_0}{D^2} J_0(2,2) = -\frac{1}{2\pi^2}.$$

We find

$$K(1,1,1;\kappa) \simeq L e^{-\kappa L}\left[\log\left(\frac{L}{a}\right) - 1\right].$$

We observe that the leading-order behavior of $K(1,1,1;\kappa) \sim L\exp(-\kappa L)$ apart from a weak logarithmic divergence coming from the δ-function nature of the intersegment repulsion ($a \to 0$). Therefore, $K(1,1,1;\kappa)T_1 \sim L\exp(-4\kappa L)$. Similarly one can show that all the terms in the above expression of $\delta_\perp^b$ has the same leading-order behavior. Using $Z = W^2(8D/\pi^2)\exp(-\kappa L)$ we find that, $\delta_\perp^b \sim (bLD/l_\parallel)\exp(-3\kappa L)$.

Within the first excited-state approximation, we can write Eq. (35) as

$$\delta_\perp^\perp = \frac{\pi^2}{16} e^{-3\kappa L} l_\perp^2 L\left(\frac{1}{l_\perp} - \frac{1}{l}\right).$$

Thus the mean field condition, $\delta_\perp = \delta_\perp^\perp + \delta_\perp^b = 0$ implies

$$l_\perp \simeq \frac{l}{2}\left[1 + \sqrt{1 - \frac{4bD}{l l_\parallel}}\right],$$

which is Eq. (15). In the limit of $D \to 0$ we can write $l_\perp \simeq l - 2bD/l_\parallel \simeq l - (4\sqrt{2\pi}/3)\sqrt{b/l}\, D^{3/2} L^{-1/2}$. Thus the leading-order behavior is $l_\perp \sim l$ with correction vanishing as $D^{3/2}$. Using this $l_\perp$ in $\kappa = (1/6) l_\perp (\pi/D)^2$, we find

$$\langle R_\perp^2\rangle \simeq \frac{D^2}{2}\left[\left(1 - \frac{8}{\pi^2}\right)\right] - \frac{D^2}{8} e^{-3\kappa L},$$

which is Eq. (17). The above expression means that, the leading-order behavior (at smallest D values) of

$$\langle R_\perp^2\rangle = \frac{D^2}{2}\left[\left(1 - \frac{8}{\pi^2}\right)\right]$$

has corrections in the next order (at larger D), which has a complicated functional dependence on intersegment interaction strength b, plate separation D and polymer contour length L.

Before ending this section, we briefly discuss the pure 2D limit of the above-mentioned calculation. The self-consistent MFT calculation for pure two dimensions leads to the mean-squared end-to-end distance

$$\langle R_{2D}^2\rangle \sim (b_0 l)^{1/2} L^{3/2}, \tag{47}$$

which obeys 2D Flory scaling. In the above expression b_0 measures the strength of the intersegment repulsion and is dimensionless, in contrast to the same parameter in three dimensions denoted by b, which has the dimension of length. This indicates that l is the only intrinsic microscopic length scale in the system. Requiring $b = b_0 l$, we find that $\langle R_\parallel^2\rangle$ reaches the 2D limit of $\langle R_{2D}^2\rangle$ when $D \sim l$ (see Appendix D).

3. *Nonmonotonicity in overall polymer size: Crossover*

Clearly, the mean-squared end-to-end distance $\langle R_{\rm tot}^2\rangle = 2\langle R_\parallel^2\rangle + \langle R_\perp^2\rangle$ should show a minimum as a function of changing plate separation D. This comes about because of the completely opposing behaviors of the two components: While the size in the confining direction $\langle R_\perp^2\rangle$ shrinks with decreasing D, the polymer size in the unconfined directions $\langle R_\parallel^2\rangle$ expands. Keeping up to the leading-order behavior in $\langle R_\perp^2\rangle$ [$= (1 - 8/\pi^2)D^2/2$] one can easily find the crossover plate separation [using Eqs. (17) and (18)]

$$D_c = (2\pi)^{-1/5}\left(1 - \frac{8}{\pi^2}\right)^{-2/5} (bl)^{1/5} L^{3/5}, \tag{48}$$

where $\langle R_{\rm tot}^2\rangle$ reaches the minimum. With enhanced degree of confinement (reduced D) the total size of the polymer $\langle R_\perp^2\rangle$ first shrinks, and when $D < D_c$ the size starts to grow.

D_c follows the same 3D Flory scaling form as the size of an excluded volume polymer freely floating in three dimensions. Thus the position of this minimum scaled by the bulk polymer size (end-to-end distance or radius of gyration) $D_c/L^{3/5}$ should be independent of polymer contour length L. The MC simulation results shown in Fig. 1 of Ref. [20] corroborate this fact.

IV. SIMULATIONS

In the previous two sections we demonstrated scaling arguments and a MFT to obtain estimates for the size and shape of confined excluded volume polymers. To validate our mean field picture, we present the results of a full numerical simulation for such a system.

A. Method

We perform molecular dynamics (MD) simulations of an excluded volume bead-spring chain trapped between two soft walls in the presence of a Langevin heat bath. All the beads interact via the fully repulsive part of shifted Lennard-Jonnes potential $V_{\rm LJ}^{\rm rep}(r) = 4\epsilon[(\sigma/r)^{12} - (\sigma/r)^6 + 1/4]$, with a cutoff distance set to $r_c = 2^{1/6}\sigma$ so that $V_{\rm LJ}^{\rm rep}(r \geqslant r_c) = 0$. Here ϵ and σ set the energy and length scales, respectively. The bond between two neighboring beads are modeled by a *shifted* harmonic potential $V_{\rm sp}(r) = (A/2)(r - \sigma)^2$ with spring constant $A = 100\epsilon/\sigma^2$ such that the equilibrium bond length, in the absence of any other forces, is σ. Here r denotes the center-to-center distance between a pair of beads. We assume that the polymer is confined within two parallel walls placed at $z = -D/2, D/2$. The repulsive potential due to the walls is assumed to be the integrated and shifted Lennard-Jones potential $V_{\rm wall}(\delta z) = \epsilon[(\sigma/\delta z)^{10} - (\sigma/\delta z)^4 + g]$ with

$g = (5/2 - 1)(2/5)^{5/3}$ and a cutoff distance $z_c = (5/2)^{1/6}\sigma$, so that $V_{\rm wall}(|\delta z| \geqslant z_c) = 0$. Here δz is the z separation of a bead from any one of the walls (top or bottom). MD simulations were performed using the standard velocity-Verlet algorithm [31] with a time step $\delta t = 0.01\tau$, where $\tau = \sigma\sqrt{m/\epsilon}$ is the characteristic timescale. We choose the mass of each bead $m = 1$. The temperature is kept constant at $T = 1.0\,\epsilon/k_B$ by using a Langevin thermostat [32] characterized by an isotropic friction coefficient $\gamma = 1/\tau$. Similar methods have been successfully used earlier for MD simulation of polymers in various contexts [24,33].

B. Results

The quantity we are interested in is the equilibrium size and shape of the polymer. In the model we simulate, the polymer is made of $i = 1, \ldots, N$ beads with a mean contour length $L = (N - 1)$ in units of σ. We follow the mean-squared end-to-end distance in the confining z direction $\langle Z^2\rangle = \langle (z_N - z_1)^2\rangle$ as well as in the unconfined xy plane $\langle X^2\rangle = \langle (x_N - x_1)^2\rangle$, $\langle Y^2\rangle = \langle (y_N - y_1)^2\rangle$. The time evolution of these quantities allows us to identify the equilibration of the system. In order to test the validity of our simulation scheme, in a separate simulation of the bulk system (using periodic boundary conditions in all three directions) we measured $\langle R^2_{\rm bulk}\rangle = \langle X^2\rangle + \langle Y^2\rangle + \langle Z^2\rangle$ as a function of polymer contour length $L = 8, 16, 32, 64, 128, 256$ to obtain Flory scaling $\langle R^2_{\rm bulk}\rangle \sim L^{6/5}$ (data not shown).

For the simulations of confined system we used an $N = 64$ bead polymer. The simulations were equilibrated for $10^6\tau$ before collecting data over further $3 \times 10^8\tau$. We used periodic boundary conditions in x and y directions with the lateral extent of the simulation box in these directions $W = 2L$. In Fig. 2 we have plotted the three components of mean-squared end-to-end distance $\langle X^2\rangle' = \langle X^2\rangle - \lambda_\parallel$, $\langle Y^2\rangle' = \langle Y^2\rangle - \lambda_\parallel$, and $\langle Z^2\rangle' = \langle Z^2\rangle + \lambda_\perp$ where $\lambda_\parallel$ and $\lambda_\perp$ are offset polymer sizes, which comes about for reasons discussed in the following.

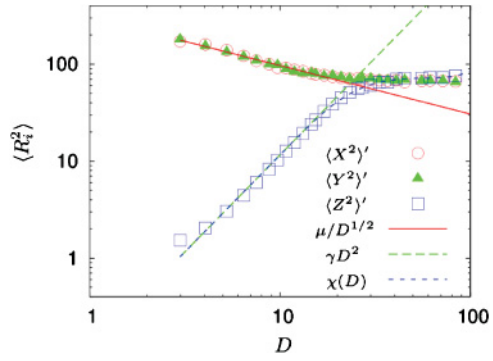

FIG. 2. (Color online) Components of mean-squared end-to-end distance $\langle R_i^2\rangle$ as a function of plate separation D. All lengths are expressed in units of σ. We have plotted the components $\langle X^2\rangle' = \langle X^2\rangle - \lambda_\parallel$, $\langle Y^2\rangle' = \langle Y^2\rangle - \lambda_\parallel$, and $\langle Z^2\rangle' = \langle Z^2\rangle + \lambda_\perp$ where $\lambda_\parallel$ and $\lambda_\perp$ are offset polymer sizes (see main text). With decreasing D, $\langle X^2\rangle$ and $\langle Y^2\rangle$ increases in the same manner while $\langle Z^2\rangle$ decreases. All the components obey de Gennes scaling, up to the leading order: $\langle X^2\rangle' = \langle Y^2\rangle' = \mu/D^{1/2}$, and $\langle Z^2\rangle' = \gamma D^2$ where $\mu = 306$ and $\gamma = 0.12$. The fitted values of offsets are $\lambda_\parallel = 12.8 \pm 4.2$ and $\lambda_\perp = 1.4$. At larger D, $\langle Z^2\rangle'$ shifts from the scaling form [Eq. (17)] as $\chi(D) = \gamma D^2 - c_1 D^2 \exp(-c_2/D^2 + c_3/D^{1/2})$ where $c_1 = 0.1, c_2 = 970$, and $c_3 = 2.06 \pm 0.36$. The fitting error in all the parameters is less than 5%, unless specified otherwise.

The mean-squared end-to-end distance in the confining direction $\langle Z^2\rangle'$ shrinks with increasing degree of confinement (decreasing D) as γD^2 (Fig. 2). Apart from an additive offset $\lambda_\perp$, this is consistent with the leading-order behavior predicted by our MFT [Eq. (17)] and de Gennes scaling. Due to a finite nonzero range of repulsion z_c coming from the soft-wall confinement (not incorporated in the MFT as in the MFT we assumed hard-wall confinement for simplicity), simulated $\langle Z^2\rangle$ gets suppressed by an extra amount $\lambda_\perp$. This indicates that $\lambda_\perp$ should be a function of z_c, which vanishes as $z_c \to 0$ (hard-wall limit). The fitting procedure in Fig. 2 gives $\lambda_\perp = 1.4 \pm 0.06$, which is numerically indistinguishable from $z_c^2 = 1.36$. At larger D, we find a saturation of $\langle Z^2\rangle$ that obeys the functional form (Fig. 2)

$$\chi(D) = \gamma D^2 - c_1 D^2 \exp(-c_2/D^2 + c_3/D^{1/2}).$$

Notice that this form of $\chi(D)$ is obtained from the expression of $\langle R_\perp^2\rangle$ obtained from Eqs. (17) and (15).

Figure 2 clearly shows that with increasing degree of confinement, the components of mean-squared end-to-end separation in the unconfined directions expands $\langle X^2\rangle' = \langle Y^2\rangle' = \mu/D^{1/2}$, in agreement with de Gennes scaling. Note that an offset like $\lambda_\parallel$ was expected from our MFT [see the first line of Eq. (18)]. Further, the excess compression of $\langle Z^2\rangle$ by $\lambda_\perp$ requires an extra bit of expansion in the parallel components. Here $\lambda_\parallel$ contains this contribution too. At large enough plate separations $\langle X^2\rangle$, $\langle Y^2\rangle$ saturate to their bulk value.

The total mean-squared end-to-end distance of the confined $\langle R^2_{\rm tot}\rangle = \langle X^2\rangle + \langle Y^2\rangle + \langle Z^2\rangle$ shows a nonmonotonic dependence on D (Fig. 3). $\langle R^2_{\rm tot}\rangle$, starting from its bulk value at large D, first reduces to reach a minimum and then expands as we reduce the plate separation. The initial decrease in size is mainly governed by the shrinkage in $\langle Z^2\rangle$. At small D values, the large increase of the polymer size in the unconfined directions $\langle X^2\rangle$ and $\langle Y^2\rangle$ takes over. The crossover between these two different behaviors takes place at the minimum of $\langle R^2_{\rm tot}\rangle$, a feature predicted by the MFT [Eq. (48)] as well as by de Gennes scaling (Sec. II). Figure 3 shows that the scaling

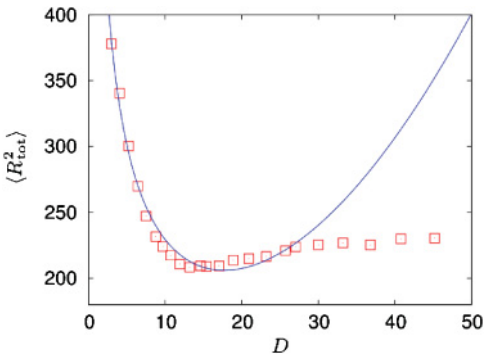

FIG. 3. (Color online) Mean squared end-to-end distance $\langle R^2_{\rm tot}\rangle = \langle X^2\rangle + \langle Y^2\rangle + \langle Z^2\rangle$ as a function of plate separation D. The line is a plot of $2(\mu/D^{1/2} + \lambda_\parallel) + (\gamma D^2 - \lambda_\perp)$ where we used the same values of μ, γ, $\lambda_\parallel$, and $\lambda_\perp$ as in Fig. 2.

forms added with the offset parameters in the three components of the mean-squared end-to-end distance does capture the nonmonotonicity as well as the approximate position of the minimum in $\langle R_{\rm tot}^2 \rangle$.

In Ref. [21] a MC simulation of self-avoiding lattice random walk confined within two parallel reflecting planes was used to show that the total 3D radius of gyration varies nonmonotonically with the separation between the reflecting planes. This behavior is similar to the nonmonotonicity we obtained for the end-to-end distance $\langle R_{\rm tot}^2 \rangle$. We have also explicitly calculated the 3D radius of gyration from our simulation (data not shown). This quantity showed the same nonmonotonic behavior as in Ref. [21]. The MFT calculation in Ref. [25] could reproduce the nonmonotonicity in 3D averaged end-to-end distance of a confined excluded volume polymer. However, Ref. [25] could not determine the components $\langle R_{\parallel}^2 \rangle$ and $\langle R_{\perp}^2 \rangle$ separately, and as a result the method could not be used to show that the nonmonotonicity in $\langle R_{\rm tot}^2 \rangle$ is actually expected from de Gennes scaling of these two components. Recently, an off-lattice MD simulation of confined excluded volume polymers explicitly verified de Gennes scaling for $\langle R_{\parallel}^2 \rangle$ and $\langle R_{\perp}^2 \rangle$ [24].

Our simulations showed that $\langle R_{\parallel}^2 \rangle$ ($\langle X^2 \rangle$, $\langle Y^2 \rangle$) and $\langle R_{\perp}^2 \rangle$ ($\langle Z^2 \rangle$) separately obey de Gennes scaling at small D limit. For $\langle R_{\perp}^2 \rangle$, we have explicitly shown that the corrections to de Gennes scaling predicted by our MFT correctly captures our simulation results. The nonmonotonicity in $\langle R_{\rm tot}^2 \rangle$ and the prediction of the minimum at a specified plate separation D as obtained from our MFT is also validated by our simulation. Moreover, the simulations clearly showed that $\langle R_{\parallel}^2 \rangle$ varies monotonically with D, in agreement with de Gennes scaling, and in contrast to experimental observations in Refs. [10,11].

V. DISCUSSION AND OUTLOOK

In this paper we have presented a mean-field approach to calculate the mean-squared end-to-end distance of a self-avoiding polymer confined between two purely repulsive parallel plates. The method allowed us to calculate all the components of this quantity separately as a function of plate separation. Up to the leading-order calculation, we recovered Flory scaling in the limit of large plate separations (bulk limit) and de Gennes scaling in the limit of small plate separations. The next to leading-order correction allows a smooth transition from de Gennes regime toward Flory regime. We believe that higher-order perturbation calculations using our MFT framework will further bridge the gap between the two regimes. We showed that the nonmonotonicity of the overall polymer size as a function of the increased degree of confinement, as clearly captured by our MFT, was already inherent to de Gennes scaling. The numerical results from MD simulations showed good agreement with our MFT predictions.

It is, however, hard to make quantitative comparisons between the theoretical calculations and the simulations for quantities such as actual prefactors of scaling laws. There are two reasons behind this. First, these nonuniversal quantities depend on the detailed nature and strength of the interactions. Second, as was already discussed in Ref. [28], the effective values of the prefactors in the scaling forms depend on up to which order the perturbative calculations are performed in the MFT.

It is important to note the simple fact that an excluded volume polymer (with repulsive intersegment interaction) confined between purely repulsive plates can only shrink in the transverse direction $R_{\perp}$ and expand in the direction parallel to the plates $R_{\parallel}$ with reducing channel width D. A linear superposition of these two monotonic but opposing features leads to nonmonotonicity in the total 3D size $\langle R_{\rm tot}^2 \rangle$. Thus, this behavior is perfectly explainable by de Gennes scaling, as was shown in Sec. II. This is the reason behind the nonmonotonicity observed for the total 3D radius of gyration obtained from earlier simulations of a repulsively confined self-avoiding polymer [20]. Note that earlier literature [20,25] failed to notice this fact and described the nonmonotonicity in the 3D radius of gyration as a behavior beyond the scope of de Gennes scaling.

Let us now briefly discuss our results vis-à-vis two recent experiments on DNA confined between parallel plates [10,11]. In Ref. [10] the average radius of gyration of confined DNA was measured from configurations projected onto a plane parallel to the confining glass plates. This experiment showed that upon reducing the plate separation D, the *projected* radius of gyration first shrank to reach a minimum before expanding in accordance with de Gennes scaling $D^{-1/4}$. A similar nonmonotonic feature in the projected size of confined DNA was reported again in a more recent experiment [11]. We emphasize that this nonmonotonicity observed in the projected size ($\sim R_{\parallel}$) should not be confused with the nonmonotonicity seen in $\langle R_{\rm tot}^2 \rangle$ (Fig. 3). The nonmonotonicity observed in $R_{\parallel}$ in experiments [10,11] is not expected from de Gennes scaling. Our MFT results agree with de Gennes scaling for very small D and allowed us to calculate corrections to de Gennes scaling for larger D. However, these corrections do not lead to nonmonotonicity in $R_{\parallel}$ (or $R_{\perp}$). Our MD simulation of a polymer made of purely repulsive segments confined within a purely repulsive channel showed good agreement with our MFT and also did not show nonmonotonicity in $R_{\parallel}$ or $R_{\perp}$ with changing D. Using our simulations, we have also evaluated the projected radius of gyration of the polymer exactly in the same manner as described in Ref. [10]. This quantity showed a clear monotonic increase with decreasing plate separation as $D^{-1/4}$ (data not shown). This is in contrast to the observed behavior in Refs. [10,11], and in agreement with our assertion that polymer size in the unconfined directions can only monotonically grow with increasing degree of confinement. The fact that both our MFT and our simulations unequivocally show that the behavior of $R_{\parallel}$ and $R_{\perp}$ of excluded volume polymers is monotonic with the channel width, and thus at variance with the experimental findings, implies that other effects must play a role.

Reference [11] speculated that the nonmonotonicity in $R_{\parallel}$ observed in experiments might be due to an effective attractive interaction between the polymer segments and the confining walls, as the detailed nature of polymer-wall interaction is both hard to control and determine in experiments. Various other factors might also impact the outcome of the experiments in a nontrivial manner; e.g., the finite focal depth of microscope used to observe the conformations (this depth is within the range of D [34] used in Ref. [10]), possibility of a nonzero

angle between the confining walls, imperfect screening of the negative charge on the DNA, accumulation of charge on the confining plates, remnant fluid flow in the flow channel used in Ref. [10], etc. It is, however, beyond the scope of the present paper to identify which conditions might have led to the nonmonotonicity observed in the experiments.

Finally, we note that the MFT approach used in this paper can be easily extended to other confining geometries, e.g., cubic or cylindrical pores. The cylindrical confinement is a natural choice for the study of bacterial chromosomes [5]. Within a biological cell, binding of proteins on DNA may enhance (or reduce) the effective persistence length of DNA. Thus it would be interesting to examine the effect of varying bending stiffness on confined polymers. A similar MFT method may potentially also be used to describe tethered polymers. For this case one may need to self-consistently determine the step size of the effective Gaussian polymer as a function of distance from the tethered end. Thus, this mean-field approach has the potential to provide analytical access to many situations of biological relevance.

ACKNOWLEDGMENTS

This work is part of the research program of the Stichting voor Fundamenteel Onderzoek der Materie (FOM), which is supported by the Nederlandse organisatie voor Wetenschappelijk Onderzoek (NWO). D.C. is funded by project 07DNAA02 in the FOM-program no. 103 "DNA in action: Physics of the genome." We thank C. Dekker for discussions on Ref. [10], and Nils Becker for a critical reading of the manuscript.

APPENDIX A: CALCULATING GREEN'S FUNCTION

A separation of variable $G_0 = f(L)\psi(\mathbf{r}_\parallel)\phi(z)$ in Eq. (20) leads to

$$\frac{1}{f}\frac{df}{dL} = \frac{l_\parallel}{6}\frac{1}{\psi}\nabla_\parallel^2\psi + \frac{l_\perp}{6}\frac{1}{\phi}\frac{d^2\phi}{dz^2} \equiv -E, \tag{A1}$$

where E is an arbitrary constant. Further, let us assume

$$\left(\frac{d^2}{dz^2} + k_z^2\right)\phi(z) = 0, \tag{A2}$$

$$(\nabla_\parallel^2 + \mathbf{k}_\parallel^2)\psi(\mathbf{r}_\parallel) = 0. \tag{A3}$$

The Dirichlet boundary condition $G_0(z = 0, D) = 0$ requires the solution $\phi_n(z) = \sqrt{2/D}\sin(k_z^n z)\sqrt{2/D}\sin(k_z^n z')$ with $k_z^n = (n\pi/D)$, n being a positive integer. The solution in the x and y directions gives $\psi(\mathbf{r}_\parallel) = \exp(i\mathbf{k}_\parallel \cdot \mathbf{r}_\parallel)$ with a continuum of $\mathbf{k}_\parallel$ modes in the presence of an open boundary condition. Equation (A1) leads to the identity

$$E = \frac{l_\parallel}{6}\mathbf{k}_\parallel^2 + \frac{l_\perp}{6}\left(\frac{n\pi}{D}\right)^2. \tag{A4}$$

Thus the solution of the differential equation Eq. (20) has the form $\exp(-EL)\exp(i\mathbf{k}_\parallel \cdot \mathbf{r}_\parallel)\sin(k_z^n z)\sin(k_z^n z')$. The general solution is obtained by summing (integrating) over all possible modes n $(\mathbf{k}_\parallel)$

$$\begin{aligned} G_0 &= \frac{2}{D}\int \frac{d\mathbf{k}_\parallel}{(2\pi)^2}\sum_{n=1}^{\infty} e^{-(l_\parallel/6)\mathbf{k}_\parallel^2 L - (l_\perp/6)(n\pi/D)^2 L} e^{i\mathbf{k}_\parallel\cdot(\mathbf{r}_\parallel - \mathbf{r}'_\parallel)} \\ &\quad \times \sin\left(\frac{n\pi}{D}z\right)\sin\left(\frac{n\pi}{D}z'\right) \\ &= \frac{3}{2\pi l_\parallel L}e^{-3(\mathbf{r}_\parallel - \mathbf{r}'_\parallel)^2/2l_\parallel L}\frac{2}{D}\sum_{n=1}^{\infty} e^{-(l_\perp/6)(n\pi/D)^2 L} \\ &\quad \times \sin\left(\frac{n\pi}{D}z\right)\sin\left(\frac{n\pi}{D}z'\right) \equiv G_\parallel\, G_\perp. \end{aligned} \tag{A5}$$

APPENDIX B: CONTRIBUTIONS FROM EXCLUDED VOLUME INTERACTIONS

In this Appendix we calculate $\delta_\parallel^b$ and $\delta_\perp^b$. The first-order contributions due to the excluded volume term in the Hamiltonian are of the form

$$\begin{aligned} &\langle A(\mathbf{r}(0),\mathbf{r}(L))\,\beta\Delta\mathcal{H}_b\rangle_0 \\ &= \frac{1}{Z}\frac{1}{2}b\int d\mathbf{r}(0)\int d\mathbf{r}(L)\,A[\mathbf{r}(0),\mathbf{r}(L)]\int_0^L ds\int_0^L ds' \\ &\quad \times \int_{\mathbf{r}(0)}^{\mathbf{r}(L)}\mathcal{D}[\mathbf{r}(s)]\delta[\mathbf{r}(s) - \mathbf{r}(s')]\exp\{-\beta\mathcal{H}_0[\mathbf{r}(s)]\} \\ &\equiv \frac{1}{Z}\frac{1}{2}b\int d\mathbf{r}(0)\int d\mathbf{r}(L)\,A[\mathbf{r}(0),\mathbf{r}(L)] \\ &\quad \times \int_0^L ds\int_0^L ds' E[s,s'|\mathbf{r}(0),\mathbf{r}(L)], \end{aligned}$$

where the integration over end points is performed for all possible $\mathbf{r}(0)$ and $\mathbf{r}(L)$. We consider the evaluation of the kernel $E(s,s'|\mathbf{r}(0),\mathbf{r}(L))$ of the inner integration, assuming for the moment that $s > s'$. The Chapman-Kolmogorov property

$$G(\mathbf{r},L|\mathbf{r}',0) = \int d\mathbf{r}'' G(\mathbf{r},L|\mathbf{r}'',L-s)\,G(\mathbf{r}'',s|\mathbf{r}',0) \tag{B1}$$

then allows us to write

$$\begin{aligned} E(s,s' \mid \mathbf{r}(\mathbf{0}),\mathbf{r}(\mathbf{L})) &= \int d\mathbf{r}'\mathbf{G_0}(\mathbf{r}(\mathbf{L}),\mathbf{L} \mid \mathbf{r}',\mathbf{s}) \\ &\quad \times G_0(\mathbf{r}',\mathbf{s} \mid \mathbf{r}',\mathbf{s}')\,\mathbf{G_0}(\mathbf{r}',\mathbf{s}' \mid \mathbf{r}(\mathbf{0}),\mathbf{0}). \end{aligned} \tag{B2}$$

We also use the fact that since the Green's function factorizes as $G_0 = G_\parallel G_\perp$, the separation of variable works for $E = E_\parallel[s,s' \mid \mathbf{r}_\parallel(0),\mathbf{r}_\parallel(L)] \times E_\perp[s,s' \mid r_\perp(0), r_\perp(L)]$ as well.

As the longitudinal part is unaffected by the constraints, it is the simplest case. Indeed, as

$$G_\parallel(\mathbf{r}',s|\mathbf{r}',s') = \frac{3}{2\pi l_\parallel(s-s')} \tag{B3}$$

does not depend on the intermediate position $\mathbf{r}'_\parallel$ we immediately find that

$$\begin{aligned} &E_\parallel[s,s' \mid \mathbf{r}_\parallel(0),\mathbf{r}_\parallel(L)] \\ &= \frac{3}{2\pi l_\parallel(s-s')}G_\parallel(\mathbf{r}_\parallel(L),L-(s-s') \mid \mathbf{r}_\parallel(0),0). \end{aligned} \tag{B4}$$

A similar simplification does not hold for the transverse component as

$$G_\perp(r'_\perp,s|r'_\perp,s') = \frac{2}{D}\sum_{n=1}^{\infty}\sin^2\left(\frac{n\pi}{D}r'_\perp\right)e^{-\kappa n^2(s-s')} \quad \text{(B5)}$$

[with $\kappa = (l_\perp/6)(\pi/D)^2$] *does* depend on $r'_\perp$. We therefore find that

$$\begin{aligned}E_\perp[s,s' \mid r_\perp(0),r_\perp(L)] &= \frac{1}{D^2}\sum_{n_L,n',n_0=1}^{\infty} e^{-\kappa L n_L^2}e^{-\kappa s(n'^2-n_L^2)}e^{-\kappa s'(n_0^2-n'^2)} \\ &\times\left[2\delta_{n_0,n_L}+\delta_{n',(n_0+nL)/2}-\delta_{n',(n_0-nL)/2}-\delta_{n',(nL-n_0)/2}\right] \\ &\times\sin\left[\frac{n_L\pi}{D}r_\perp(L)\right]\sin\left[\frac{n_0\pi}{D}r_\perp(0)\right]. \quad \text{(B6)}\end{aligned}$$

Again, we can write

$$\begin{aligned}\langle R_\parallel^2\beta\Delta\mathcal{H}_b\rangle_0 &= Z^{-1}\frac{1}{2}b\int_0^L ds\int_0^L ds'\int d\mathbf{r}(\mathbf{0})\int \mathbf{dr}(\mathbf{L}) \\ &\times[\mathbf{r}_\parallel(L)-\mathbf{r}_\parallel(0)]^2E(s,s' \mid \mathbf{r}(\mathbf{0}),\mathbf{r}(\mathbf{L})) \\ &= Z^{-1}\frac{1}{2}b\int_0^L ds\int_0^L ds' \\ &\times\left\{\int d\mathbf{r}_\parallel(0)\int d\mathbf{r}_\parallel(L)[\mathbf{r}_\parallel(L)-\mathbf{r}_\parallel(0)]^2E_\parallel\right\} \\ &\times\left\{\int dr_\perp(0)\int dr_\perp(L)E_\perp\right\} \\ &\equiv Z^{-1}\frac{1}{2}b\int_0^L ds\int_0^L ds' I_\parallel^2(s,s')I_\perp^0(s,s'). \quad \text{(B7)}\end{aligned}$$

Similarly,

$$\langle R_\perp^2\beta\Delta\mathcal{H}_b\rangle_0 = Z^{-1}\frac{1}{2}b\int_0^L ds\int_0^L ds' I_\parallel^0(s,s')I_\perp^2(s,s'), \quad \text{(B8)}$$

$$\langle\beta\Delta\mathcal{H}_b\rangle_0 = Z^{-1}\frac{1}{2}b\int_0^L ds\int_0^L ds' I_\parallel^0(s,s')I_\perp^0(s,s'). \quad \text{(B9)}$$

In the above, we used the definitions

$$I_\parallel^0(s,s') = \int d\mathbf{r}_\parallel(0)\int d\mathbf{r}_\parallel(L)E_\parallel[s,s' \mid \mathbf{r}_\parallel(0),\mathbf{r}_\parallel(L)], \quad \text{(B10)}$$

$$\begin{aligned}I_\parallel^2(s,s') &= \int d\mathbf{r}_\parallel(0)\int d\mathbf{r}_\parallel(L)E_\parallel[s,s' \mid \mathbf{r}_\parallel(0),\mathbf{r}_\parallel(L)] \\ &\times[\mathbf{r}_\parallel(L)-\mathbf{r}_\parallel(0)]^2, \quad \text{(B11)}\end{aligned}$$

$$I_\perp^0(s,s') = \int dr_\perp(0)\int dr_\perp(L)E_\perp[s,s' \mid r_\perp(0),r_\perp(L)], \quad \text{(B12)}$$

$$\begin{aligned}I_\perp^2(s,s') &= \int dr_\perp(0)\int dr_\perp(L)E_\perp[s,s' \mid r_\perp(0),r_\perp(L)] \\ &\times[r_\perp(L)-r_\perp(0)]^2. \quad \text{(B13)}\end{aligned}$$

We can now evaluate the integrals over the end points. The longitudinal ones are easier to compute:

$$\begin{aligned}I_\parallel^0(s,s') &= W^2\frac{3}{2\pi l_\parallel(s-s')}, \\ I_\parallel^2(s,s') &= W^2\frac{3}{2\pi l_\parallel(s-s')}\times\frac{2}{3}l_\parallel[L-(s-s')]. \quad \text{(B14)}\end{aligned}$$

The only $r_\perp(0)$ and $r_\perp(L)$-dependent term present in $E_\perp[s,s' \mid r_\perp(0),r_\perp(L)]$ is $q[r_\perp(L),r_\perp(0)] = \sin[n_L\pi r_\perp(L)/D]\times\sin[n_0\pi r_\perp(0)/D]$. To evaluate the integration in $I_\perp^0(s,s')$ we use the identity

$$\int_0^D dr_\perp\sin\left(\frac{n\pi}{D}r_\perp\right) = \frac{D}{n\pi}[1-(-1)^n]. \quad \text{(B15)}$$

Thus,

$$\begin{aligned}I_\perp^0(s,s') &= \sum_{n_L,n',n_0=1}^{\infty} e^{-\kappa L n_L^2}e^{-\kappa s(n'^2-n_L^2)}e^{-\kappa s'(n_0^2-n'^2)} \\ &\times\left[2\delta_{n_0,n_L}+\delta_{n',(n_0+n_L)/2}\right. \\ &\left.-\delta_{n',(n_0-n_L)/2}-\delta_{n',(n_L-n_0)/2}\right]J_0(n_L,n_0), \quad \text{(B16)}\end{aligned}$$

where

$$J_0(n_L,n_0) = \frac{1}{n_0n_L\pi^2}[1-(-1)^{n_L}][1-(-1)^{n_0}]. \quad \text{(B17)}$$

To calculate $I_\perp^2(s,s')$ one requires to use the integration of sine function with powers, such as, $\int_0^D dr\,\sin(n\pi r/D)$, $\int_0^D dr\,r\,\sin(n\pi r/D)$, and $\int_0^D dr\,r^2\,\sin(n\pi r/D)$. This gives us

$$\begin{aligned}I_\perp^2(s,s') &= D^2\sum_{n_L,n',n_0=1}^{\infty} e^{-\kappa L n_L^2}e^{-\kappa s(n'^2-n_L^2)}e^{-\kappa s'(n_0^2-n'^2)} \\ &\times\left[2\delta_{n_0,n_L}+\delta_{n',(n_0+nL)/2}-\delta_{n',(n_0-nL)/2}\right. \\ &\left.-\delta_{n',(nL-n_0)/2}\right]J(n_L,n_0), \quad \text{(B18)}\end{aligned}$$

where

$$\begin{aligned}J(n_L,n_0) &= -\frac{1}{n_L^3n_0\pi^4}\{(-1)^{n_L}n_L^2\pi^2+2[1-(-1)^{n_L}]\} \\ &\times[1-(-1)^{n_0}]-\frac{2}{n_Ln_0\pi^2}(-1)^{n_0}(-1)^{n_L} \\ &-\frac{1}{n_Ln_0^3\pi^4}\left[(-1)^{n_0}n_0^2\pi^2+2(1-(-1)^{n_0})\right] \\ &\times[1-(-1)^{n_L}]. \quad \text{(B19)}\end{aligned}$$

We used $s > s'$ above. Now, using the identity

$$\frac{1}{2}\int_0^L ds\int_0^L ds' = \int_0^L ds'\int_{s'}^L ds, \quad \text{(B20)}$$

we have

$$\delta_\parallel^b = Z^{-1}b\int_0^L ds'\int_{s'}^L ds I_\perp^0(s,s')[I_\parallel^2(s,s')-\langle R_\parallel^2\rangle_0 I_\parallel^0(s,s')], \quad \text{(B21)}$$

$$\delta_\perp^b = Z^{-1}b\int_0^L ds'\int_{s'}^L ds I_\parallel^0(s,s')[I_\perp^2(s,s')-\langle R_\perp^2\rangle_0 I_\perp^0(s,s')]. \quad \text{(B22)}$$

We now have all the ingredients to calculate the perturbation corrections.

A. Parallel component $\delta_\parallel^b$

We have

$$[I_\parallel^2(s,s') - \langle R_\parallel^2\rangle_0 I_\parallel^0(s,s')] = \frac{3W^2}{2\pi l_\parallel (s-s')} \times \left\{ \frac{2}{3} l_\parallel [L-(s-s')] - \frac{2}{3} l_\parallel L \right\} = -\frac{W^2}{\pi}. \tag{B23}$$

Thus in evaluating the integral in $\delta_\parallel^b$ [Eq. ((B21)], we need to do the following integration:

$$M = e^{-\kappa L n_L^2} \int_0^L ds' \int_{s'}^L ds e^{-\kappa s(n'^2-n_L^2)} e^{-\kappa s'(n_0^2-n'^2)}, \tag{B24}$$

where the only function of (s,s') in the integrand comes from $I_\perp^0(s,s')$.

Thus, we obtain

$$\delta_\parallel^b = -\frac{b}{Z} W^2 \frac{1}{\pi} \sum_{n_L,n',n_0=1}^{\infty} M(n_L,n',n_0;\kappa) \times \left[2\delta_{n_0,n_L} + \delta_{n',(n_0+nL)/2} - \delta_{n',(n_0-nL)/2} - \delta_{n',(nL-n_0)/2} \right] J_0(n_L,n_0),$$

i.e., Eq. (36).

B. Perpendicular component $\delta_\perp^b$

The only function of (s,s') in Eq. (B22) is $\exp[-\kappa s(n'^2 - n_L^2)] \exp[-\kappa s'(n_0^2 - n'^2)]$ due to the function $[I_\perp^2(s,s') - \langle R_\perp^2\rangle_0 I_\perp^0(s,s')]$ and $1/(s-s')$ due to $I_\parallel^0(s,s')$. Thus we have to evaluate the integration

$$K = e^{-\kappa L n_L^2} \int_0^L ds' \int_{s'}^L ds \frac{e^{-\kappa s(n'^2-n_L^2)} e^{-\kappa s'(n_0^2-n'^2)}}{(s-s')}. \tag{B25}$$

The term by term calculation of this quantity for each (n_0,n',n_l) encounters a pole at $s = s'$. To avoid the pole, the integration to evaluate Eq. (B25) can be rewritten as

$$K(n_L,n',n_0;\kappa) = e^{-\kappa L n_L^2} \lim_{a\to 0} \int_0^L ds' \int_{s'}^L ds \times \left[\frac{e^{-\kappa s(n'^2-n_L^2)} e^{-\kappa s'(n_0^2-n'^2)}}{(s-s')+a} \right]. \tag{B26}$$

Note that this is equivalent to replacing the delta-function overlap interaction by its Gaussian representation but keeping a nonzero variance a^2. Thus we obtain the expression (Eq. (39))

$$\delta_\perp^b = \frac{b}{Z} W^2 \frac{3}{2\pi l_\parallel} \sum_{n_L,n',n_0=1}^{\infty} D^2 K(n_L,n',n_0;\kappa) \times \left[2\delta_{n_0,n_L} + \delta_{n',(n_0+nL)/2} - \delta_{n',(n_0-nL)/2} - \delta_{n',(nL-n_0)/2} \right] \times \left[J(n_L,n_0) - \frac{\langle R_\perp^2\rangle_0}{D^2} J_0(n_L,n_0) \right].$$

APPENDIX C: BULK LIMIT OF $D \to \infty$

In this Appendix we calculate $\delta_\parallel^b$, $\delta_\perp^b$ and $\delta_\perp^\perp$ in the bulk limit of $D \to \infty$.

It is clear that, since in this limit $G_\perp$ itself is independent of D, $\delta_\parallel^b$ and $\delta_\perp^b$ are also independent of D. Using the continuum approach at $D \to \infty$,

$$E_\perp = \sqrt{\frac{3}{2\pi l_\perp (s-s')}} G_\perp(z(L),L-(s-s') \mid z(0),0) = \sqrt{\frac{3}{2\pi l_\perp (s-s')}} \times \sqrt{\frac{3}{2\pi l_\perp [L-(s-s')]}} \times \exp\left\{ -\frac{3}{2} \frac{[z(L)-z(0)]^2}{l_\perp [L-(s-s')]} \right\}. \tag{C1}$$

Then using Eq. (B12) we get

$$I_\perp^0(s,s') = \int dz(0) \int dz(L) E_\perp[s,s' \mid r_\perp(0), r_\perp(L)] = D\sqrt{\frac{3}{2\pi l_\perp (s-s')}}. \tag{C2}$$

Remember that, now, the orthogonal component of partition function has also been redefined to $Z_\perp = D$. Then using Eq. (B21),

$$\delta_\parallel^b = Z^{-1} b \int_0^L ds' \int_{s'}^L ds I_\perp^0(s,s')[I_\parallel^2(s,s') - \langle R_\parallel^2\rangle_0 I_\parallel^0(s,s')] = (W^2 D)^{-1} b(-W^2/\pi)\, D\sqrt{\frac{3}{2\pi l_\perp}} \int_0^L ds' \int_{s'}^L ds \sqrt{\frac{1}{(s-s')}} = -\frac{b}{\pi} \times \sqrt{\frac{3}{2\pi l_\perp}} \times \frac{4}{3} L^{3/2}; \tag{C3}$$

where we also used Eqs. (B14) and (27). Using Eq. (B13) we find

$$I_\perp^2(s,s') = \int_{-\infty}^{\infty} dz(0) \int_{-\infty}^{\infty} dz(L) \sqrt{\frac{3}{2\pi l_\perp (s-s')}} \times \sqrt{\frac{3}{2\pi l_\perp [L-(s-s')]}} e^{-\frac{3(z(L)-z(0))^2}{2l_\perp (L-(s-s'))}} = \sqrt{\frac{3}{2\pi l_\perp (s-s')}} D \frac{l_\perp [L-(s-s')]}{3}, \tag{C4}$$

and using Eq. (28) we get

$$\langle R_\perp^2\rangle_0 = \frac{\int_{-\infty}^{\infty} dz \int_{-\infty}^{\infty} dz' (z-z')^2 e^{-\frac{3(z(L)-z(0))^2}{2l_\perp L}}}{\int_{-\infty}^{\infty} dz \int_{-\infty}^{\infty} dz' e^{-\frac{3(z(L)-z(0))^2}{2l_\perp L}}} = \frac{l_\perp L}{3}. \tag{C5}$$

Therefore,

$$I_\perp^2(s,s') - \langle R_\perp^2\rangle_0 I_\perp^0(s,s') = -D\frac{l_\perp}{6\pi}(s-s')^{1/2}, \tag{C6}$$

and

$$I_{\parallel}^{0}(s,s')[I_{\perp}^{2}(s,s') - \langle R_{\perp}^{2}\rangle_{0} I_{\perp}^{0}(s,s')] = -W^{2}\frac{3}{2\pi l_{\parallel}(s-s')} D\sqrt{\frac{l_{\perp}}{6\pi}}(s-s')^{1/2} - W^{2}\frac{D l_{\perp}^{1/2}}{l_{\parallel}}(s-s')^{-1/2}. \quad \text{(C7)}$$

Since in this limit $Z = W^2 D$, using Eq. (B22) we find

$$\delta_{\perp}^{b} = Z^{-1} b \int_{0}^{L} ds' \int_{s'}^{L} ds I_{\parallel}^{0}(s,s')[I_{\perp}^{2}(s,s') - \langle R_{\perp}^{2}\rangle_{0} I_{\perp}^{0}(s,s')] \simeq -\frac{b l_{\perp}^{1/2}}{l_{\parallel}} L^{3/2}. \quad \text{(C8)}$$

Similarly, using Eq. (C5) in Eq. (34), we obtain

$$\delta_{\perp}^{\perp} = -\frac{3}{2}\left(\frac{1}{l} - \frac{1}{l_{\perp}}\right)\frac{\partial}{\partial \alpha_{\perp}}\langle R_{\perp}^{2}\rangle_{0} = \frac{1}{3}\left(\frac{1}{l} - \frac{1}{l_{\perp}}\right) L l_{\perp}^{2}. \quad \text{(C9)}$$

APPENDIX D: 2D LIMIT OF CONFINED SYSTEM

In pure two dimensions, the perturbative contribution due to the intersegment interactions takes the form

$$\delta_{2D}^{b} = Z_{2D}^{-1} b_0 \int_{0}^{L} ds' \int_{s'}^{L} ds [I_{\parallel}^{2}(s,s') - \langle R_{\parallel}^{2}\rangle_{0} I_{\parallel}^{0}(s,s')],$$

where $Z_{2D} = W^2$. Thus,

$$\delta_{2D}^{b} = -\frac{b_0}{2\pi} L^2,$$

where b_0 plays the role of interaction strength. Thus, $\delta_{\parallel} = \delta_{\parallel}^{\parallel} + \delta_{\parallel}^{b} = 0$ implies

$$\frac{L l_{2D}^{2}}{l} \sim \frac{b_0}{2\pi} L^2 \quad \text{or} \quad l_{2D} \sim (b_0 l)^{1/2} L^{1/2},$$

which leads to the scaling form,

$$\langle R_{2D}^{2}\rangle \sim L l_{2D} \sim (b_0 l)^{1/2} L^{3/2}. \quad \text{(D1)}$$

We expect that the polymer would behave like a pure 2D polymer in the limit of extremely small plate separation D. This limit is achieved when $\langle R_{\parallel}^{2}\rangle = \langle R_{2D}^{2}\rangle$. We have seen that the strength of the interaction b in three dimensions has the dimension of length, whereas the same strength b_0 is dimensionless in two dimensions. This shows that the only intrinsic microscopic length scale in the system is segment length l. Thus we need to express $b = b_0 l$ to search for the pure 2D limit of confined systems. With this substitution,

$$\langle R_{\parallel}^{2}\rangle \sim (b_0 l)^{1/2} L^{3/2}\left(\frac{l}{D}\right)^{1/2}. \quad \text{(D2)}$$

Therefore, $\langle R_{\parallel}^{2}\rangle$ equates $\langle R_{2D}^{2}\rangle$ when $D \sim l$, i.e., when the plate separation D becomes as small as the polymer segment length l.

[1] M. C. Lagomarsino, C. Tanase, J. W. Vos, A. M. C. Emons, B. M. Mulder, and M. Dogterom, Biophys. J. **92**, 1046 (2007).

[2] D. N. Fuller, J. P. Rickgauer, P. J. Jardine, S. Grimes, D. L. Anderson, and D. E. Smith, Proc. Natl. Acad. Sci. USA **104**, 11245 (2007).

[3] N. Kleckner, D. Zickler, G. F. Jones, J. Dekker, R. Padmore, J. Henle, and J. Hutchinson, Proc. Natl. Acad. Sci. USA **101**, 12592 (2004).

[4] D. Bates and N. Kleckner, Cell **121**, 899 (2005).

[5] S. Jun and B. Mulder, Proc. Natl. Acad. Sci. USA **103**, 12388 (2006).

[6] Y. Liu and B. Chakraborty, e-print arXiv:0906.4023.

[7] P.-G. de Gennes, *Scaling Concepts in Polymer Physics* (Cornell University Press, Ithaca, NY, 1979).

[8] Y.-L. Chen, M. D. Graham, J. J. de Pablo, G. C. Randall, M. Gupta, and P. S. Doyle, Phys. Rev. E **70**, 060901 (2004).

[9] K. Jo, D. M. Dhingra, T. Odijk, J. J. de Pablo, M. D. Graham, R. Runnheim, D. Forrest, and D. C. Schwartz, Proc. Natl. Acad. Sci. USA **104**, 2673 (2007).

[10] D. J. Bonthuis, C. Meyer, D. Stein, and C. Dekker, Phys. Rev. Lett. **101**, 108303 (2008).

[11] H. Uemura, M. Ichikawa, and Y. Kimura, Phys. Rev. E **81**, 051801 (2010).

[12] J. O. Tegenfeldt *et al.*, Proc. Natl. Acad. Sci. USA **101**, 10979 (2004).

[13] W. Reisner, K. J. Morton, R. Riehn, Y. M. Wang, Z. Yu, M. Rosen, J. C. Sturm, S. Y. Chou, E. Frey, and R. H. Austin, Phys. Rev. Lett. **94**, 196101 (2005).

[14] D. Stein, F. H. J. van der Heyden, W. J. A. Koopmans, and C. Dekker, Proc. Natl. Acad. Sci. USA **103**, 15853 (2006).

[15] M. Daoud and P.-G. de Gennes, J. Phys. (France) **38**, 85 (1977).

[16] F. Brochard and P. G. de Gennes, J. Phys. France Lett. **40**, 399 (1979).

[17] Z.-G. Wang, A. M. Nemirovsky, and K. F. Freed, J. Chem. Phys. **86**, 4266 (1987).

[18] D. Romeis and Z. Usatenko, Phys. Rev. E **80**, 041802 (2009).

[19] F. Schlesener, A. Hanke, R. Klimpel, and S. Dietrich, Phys. Rev. E **63**, 041803 (2001).

[20] J. H. van Vliet and G. ten Brinke, J. Chem. Phys. **93**, 1436 (1990).

[21] J. H. van Vliet, M. C. Luyten, and G. ten Brinke, Macromolecules **25**, 3802 (1992).

[22] S. Jun, D. Thirumalai, and B.-Y. Ha, Phys. Rev. Lett. **101**, 138101 (2008).

[23] Y. Jung, S. Jun, and B.-Y. Ha, Phys. Rev. E **79**, 061912 (2009).

[24] D. I. Dimitrov, A. Milchev, K. Binder, L. I. Klushin, and A. M. Skvortsov, J. Chem. Phys. **128**, 234902 (2008).

[25] C. E. Cordeiro, M. Molisana, and D. Thirumalai, J. Phys. II (France) **7**, 433 (1997).

[26] D. W. Schaefer, J. F. Joanny, and P. Pincus, Macromolecules **13**, 1280 (1980).

[27] P. J. Flory, *Principles of Polymer Chemistry* (Cornell University Press, Ithaca, NY, 1953).
[28] S. F. Edwards and P. Singh, J. Chem. Soc. Faraday Trans. **75**, 1001 (1979).
[29] G. Morrison and D. Thirumalai, J. Chem. Phys. **122**, 194907 (2005).
[30] M. Doi and S. F. Edwards, *The Theory of Polymer Dynamics* (Oxford University Press, New York, 1994).
[31] D. Frenkel and B. Smit, *Understanding Molecular Simulation: From Algorithms to Applications* (Academic Press, New York, 2002).
[32] G. S. Grest and K. Kremer, Phys. Rev. A **33**, 3628 (1986).
[33] B. Duenweg, M. Stevens, and K. Kremer, in *Monte Carlo and Molecular Dynamics Simulations in Polymer Science*, edited by K. Binder (Oxford University Press, New York, 1995).
[34] C. Dekker (private communication).